Geoinformatics & Geostatistics: An Overview

Research Article

A SCITECHNOL JOURNAL

Evidence of Elliptical Intrusions and Sr, Hf, Pb and O-H Isotopes of the Khanbogd Alkali Granite Pluton: Construction of Underplating Magma Associated with The Duplex Thrust

Dash Batulzii[1], Serjlkhumbe Amaramgalan[2*], Holk Gregory[3], Davaa Khishigsuren[1], Jargal Lkhamsuren[1] and Otgonhuu Javkhlan[1]

[1]*School of Geology and Mining Engineering, Mongolian University Science and Technology, Ulan Bator, Mongolia*

[2]*Rio Tinto, South Jordan, Utah, United States of America*

[3]*Department of Geology, Californian State University, Long Beach, California, United States of America*

***Corresponding Author:** Serjlkhumbe Amaramgalan, Rio Tinto, South Jordan, Utah, United States of America; E-mail: amaramgalans@riotinto.com

Received date: 09 September, 2024, Manuscript No. GIGS-24-147609;

Editor Assigned date: 11 September, 2024, PreQC No. GIGS-24-147609 (PQ);

Reviewed date: 25 September, 2024, QC No. GIGS-24-147609;

Revised date: 02 October, 2024, Manuscript No. GIGS-24-147609 (R);

Published date: 09 October, 2024, DOI: 10 .4172/2327-4581.1000410.

Abstract

The Khanbogd peralkaline granite pluton, occupying more than 1000 km^2, is located in southern Mongolia. Previously, two magmatic bodies called Western and Eastern and the flattened shape of this pluton were discovered. Several elliptical intrusions within the pluton have been detected in Landsat satellite images. These are at least four elliptical intrusions in the Western and two intrusions in the Eastern body. The granites of the inferred intrusions differed in Alumina Saturation Index (ASI) and Cross, Iddings, Pirrson and Washington (CIPW), $^{87}Sr/^{86}Sri$ and $\delta^{18}O$ values. Fe-Mg minerals in studied granites are garnet, aegirine and arfvedsonites. The low dD values (-155% to -170%) of arfvedsonite support the argument for meteoric fluid involvement in the crystallization source. Two stages of aegirine crystallization were determined before and later arfvedsonite, which formed from a phase induced by meteoric water. The domain structure of arfvedsonite indicates its crystallization from a new lagging phase, which is similar to a peritectic phase. However, the peritectoid-like system is suggested for garnet and aegirine-I. Stage II aegirine, which appeared after arfvedsonite, shows its crystallization caused by a change in magnetization when the water is exhausted in the solidus. The diffusion effect, represented by the droplets of arfvedsonite and II stage aegirine in K-feldspar followed the processes. Further, meteoric fluids resulted in disequilibrium $\delta^{18}O$ values between quartz and feldspar, which occurred in the post-solidus state. Accordingly, the K-feldspar surface has effects, such as fractured and stippled. Two adjacent intrusive bodies and undeformed host rocks at the front part of the pluton are consistent with underplating magmatic factors during duplex-type thrusting. Another factor is the multiple sources for the melt: mantle, reworked seafloor and arc rocks, which are identified by the ratio of $^{87}Sr/^{86}Sri$ and $\delta^{18}Oqz$ values. An underplate magma source is a suitable interpretation explaining the principles of low non-stable isotopes for alkali granites.

Keywords: Alkali granite; Elliptic shape; $\delta^{18}O$ isotope; Domain structure, Lagging phase, Peritectic, Duplex thrust; Underplating.

Introduction

It is widely recognized that the geology of Mongolia is characterized by the accretion of arc complexes, which is accompanied by the emplacement of voluminous calc-alkaline granites into the arc [1]. However, anorogenic alkaline granites and syenite intrusions occur in Mongolia. One of them is the Khanbogd alkaline-granite pluton, consisting of aegirine-arfvedsonite, ferro-edenite granites, pegmatites and dikes of ekerite, comendite and pantellerite. Petrogenetic models involving a mantle source have mainly been proposed for the origin of alkaline granites. The models include:

i. Fractionation of mantle-derived magmas with or without interaction of crustal rocks [2-5].

ii. Partial melting of residue from i-type granites [6,7].

iii. Crustal melting accompanied by an influx of mantle fluids [8].

iv. Vapor absent dehydration melting from tonalite and biotite-amphibole gneiss [9,10].

v. Partial melting of metasomatically altered crustal source rocks [11-13].

vi. Partial melting of lower crustal basalt and lithospheric mantle induced by a rising plume [14,15].

This model is based on research on peralkaline granites in central Mongolia. Bonin's hypothesis was different in that it assumed an underplating magmatic process for the origin of alkaline granites [16].

Vladykin et al., argued for model (i) for the origin of the Khanbogd plutonic complex. A more complete data set was used by Kovalenko et al. and they suggested a magma source from the melt *via* interactions of enriched, depleted mantle and crust materials [17-19].

The main goal of this study is to identify the features of alkaline granites in a flattened form intrusion, implying the nature of thrust faults. For this purpose, unpublished geochemical and radiogenic isotope data from Serjlkhumbe were used [20,21]. To integrate new chemical analysis with geological observations, we began to interpret 'Landsat' satellite images of the Khanbogd pluton. We have interpreted several elliptical incursions within two bodies that

previous researchers have called the Western and Eastern bodies. The sample positions allowed us to examine chemical and isotopic data interpreted intrusions.

The flattened shape of this pluton and the O and H isotope data allowed us to accept the thrust-related magma model, which involves the melting of the mantle, oceanic crust and reworked arc rocks. The low dD values (-155% to -170%) of arfvedsonite support the argument for meteoric fluid involvement in the crystallization [22-26]. Plutonic rocks crystallized at shallow crustal depths are highly susceptible to interactions with meteoric-hydrothermal fluids, resulting in quartz-feldspar pairs out of oxygen isotope equilibrium and hydrogen isotope values below those in equilibrium with magmas [27,28].

Joekar-Niasar et al., supposed that the equilibrium change is an effect of the appearance of new phases like diffusion and their lagging behind the main crystallization. They note that the domain structure expresses the coexistence of lagging and main phase minerals because of different magnetization. We established this structure in studied granites [29].

Therefore, this manuscript presents our interpretation of satellite images of the Khanbogd pluton, petrographic, geochemical and isotopic data (Sr, Nd, Hf, Pb, O and H) of alkaline granites, as well as a new model of the Khanbogd pluton.

Materials and Methods

Mineral $\delta^{18}O$ values were measured using the Thermo Finnigan Delta Plus-XP mass spectrometer at California State University, Long Beach. A modified version of the laser fluorination method of Sharp and the TC/EA method of Sharp et al., was employed for the acquisition of mineral $\delta^{18}O$ and D values, respectively [23,24]. Analytical precision and accuracy for hydrogen and oxygen (dD ± 2.0% and $\delta^{18}O$ ± 0.2%) isotopes were determined using the NBS-30 biotite (dD = -65.7%) and Caltech Rose Quartz ($\delta^{18}O$ = +8.45%) standards and reported relative to V-SMOW [30,31]. Whole rock major and 14 trace element (Ba, Ce, Cr, Ga, Nb, Ni, Pb, Rb, Sc, Sr, Th, V, Y, Zr) concentrations for 35 samples were analyzed by Rigaku RIX-2000 wavelength-depressive XRF spectrometer at Shimane University, e.g., [21]. REEs, Cs, Rb, Ba, Sr, Th, U, Nb, Ta, Pb, Zr, Hf, Li and Y analyses were carried out for selected samples by ICP-MS (Thermo ELEMENTAL, VGPQ3 at Shimane University), following the method described by Kimura et al. [32]. Sr and Nd isotopic ratios were determined for 36 samples by thermal ionization mass spectrometry (MAT262) at Shimane University, following the methods described in [33,34]. The isotopic compositions were measured in jumping multi-collection mode. The Sr isotope ratios of standard sample NBS987 (SrCO3) were used during the analysis. The isotope dilution method determined Sr isotope compositions and age dating due to the high Rb/Sr values and much lower average Sr concentrations (<10 ppm) of the Khanbogd plutonic complex. Samples were mixed with spike solution ($^{87}Rb/^{86}Sr$ mixed spike, previously prepared at Shimane University of Japan). For the interpretation of the geological setting of Khanbogd pluton, 2-3-4, 4-5-1, 5-3-2 and 7-4-1 spectral bands image LandsatTM were used. The Nikon Eclipse 50iPol microscope was used for petrography research.

Geological background of the studied Khanbogd alkali granite pluton and its surroundings

The studied Khanbogd pluton is located near the southern border of Mongolia. This pluton intruded into a lower carboniferous sedimentary basin filled by the volcano-sedimentary strata e.g. [17,19]. According to the terrane-tectonic concept, this basin is located in the Gurvansaikhan terrane, e.g., (Figure 1) [35-37].

Geological and mineralogical studies of previous researchers of the Khanbogd alkali granite pluton: Detailed mineralogical, geochemical, petrological and geophysical studies of alkaline granites of the Khanbogd pluton were carried out between 1970-1980. Aegirine-arfvedsonite, aegirine granites, dikes of various compositions and rare-earth pegmatites were identified in two neighboring ring-shaped intrusive bodies; named Eastern and Western. Modeling of gravity data suggests a flattened shape for the Khanbogd complex. The 300 km^3 Eastern body comprises medium-to fine-grained aegirine granite and is younger than the Western body. The 1000 km^3 Western body is comprised of medium-to coarse-grained aegirine-arfvedsonite granites and small bodies of red granite that lack aegirine and arfvedsonite, but contain ferro-edenite.

Numerous REE-bearing pegmatites and various compositions of dikes, such as ekerite, pantellerite and comendites were discovered in the pluton. Elpidite ($Na_2Zr_6Si_6O_{15}H_2O$) is a unique accessory mineral in these granites and pegmatites, e.g., [17]. Vladykin et al., discovered new zirconium oxide minerals from this pluton, such as armstrongite ($CaZrSi_6O_{15}$ $3H_2O$) and mongolite ($Na_2ZrSi_6O_{15}$ $3H_2O$) in pegmatites. Kynicky et al., contributed to the study of REE-bearing minerals in pegmatites [38,39].

Granites of the western body have U/Pb zircon ages of 291 ± 1 to 290 ± 1 Ma and a Rb/Sr age of 287 ± 3 Ma [19]. However, other studies produced Rb/Sr ages 295-292 Ma from aegirine-arfvedsonite granites of the Western Body, granites of both bodies and dikes. Lower to upper cretaceous red-bed continental sediments overlay Carboniferous, a bimodal basalt-comendite volcanic suite and Khanbogd pluton of Early Permian [40-43].

In the basin, where the Khanbogd pluton is located, leucogranites that analogs of felsic lavas of the bimodal volcanic suite are widespread. The U/Pb zircon age of a biotitic leucogranite near Khanbogd is 290 ± 1 Ma and the Rb/Sr whole-rock age of felsic volcanic is 291 ± 4 Ma. These emplacement ages between alkali granites, leucogranite and pantellerite indicate they are of coeval ages.

Interpretation of Landsat satellite images and the elliptic intrusions of alkaline granites in the Khanbogd pluton: We used a combination of 'Landsat' spectral bands 2-3-4, 4-5-1, 5-3-2 and 7-4-1 to interpret the geological setting of the Khanbogd pluton. Four shapes, identical to the phases, are represented by different color images across the western body. The yellowish, pale red-pinkish, bluish and pale pinkish color tones are reflected from an arc-shaped stripe along the outer edge of the Western body (Figure 2).

This is marked I-W in Figure 2, which defines the first intrusion of the Western body. An elliptical shape with pale blue, blue, brown and pale red reflected color tones inside the arcuate strip is denoted as unit II-W. A narrow blackish zone is distinguished between an elliptical (II-W) and an arcuate (I-W) shape. This zone represents uplifted country rocks and marks the boundary of two granite intrusions I-W and II-W. The smaller irregular shape, displaying dark and pale blue, brown and bright reddish colors is the next phase in the relationship and is noted III-W.

Images marked IV-W refer to small intrusions of ferro-edenite granites. Ferro-edinite granite dikes are common in II-W and III-W. Satellite images display a sharp contact between the western and eastern intrusive bodies. The cross-cutting relationships between granites indicate that the small elliptical Eastern body is younger than the Western body. Contrasting colors in the small body suggest there are two intrusions in the Eastern body marked as the I-E and II-E. The granites I-E, which occupy most of the eastern body are indicated by lighter colors. The II-E is characterized by its smaller size and blackish color. Interpreted elliptical intrusions in the studied Khanbogd pluton are shown in Figure 2e.

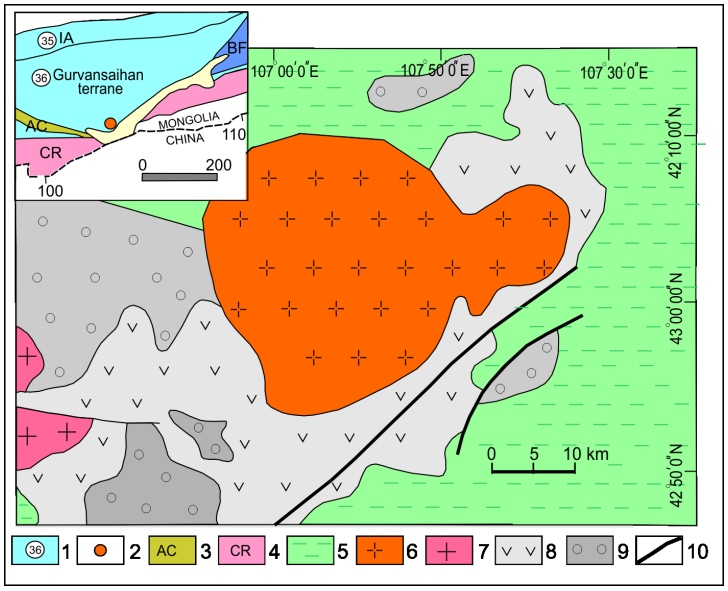

Figure 1: Location of the Khanbogd peralkaline granite pluton in the terrane-tectonic scheme of Mongolia and its surrounding geological formations. Modified from [84, 1]. Terranes (1-4) per Badarch et al. [1]**.**

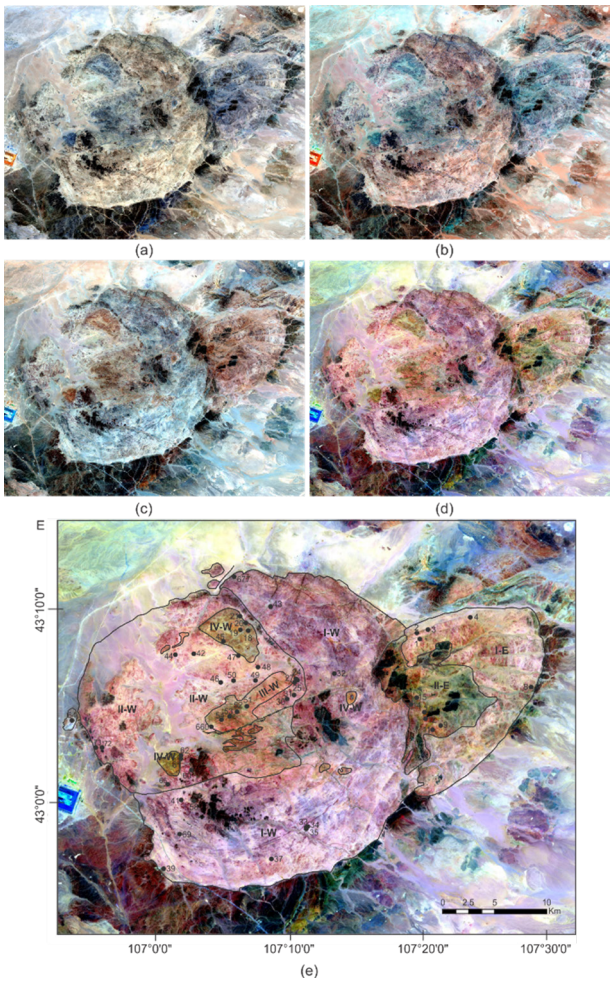

Figure 2: Images of the Khanbogd granite pluton in the landsat bands and an interpreted intrusion using them landsat bands. **Note:** (a) -/2-3-4/; (b) -/4-5-1/; (c) -/5-3-2/; (d) -/7-4-1/; (e) interpreted elliptical intrusions and sample points (Interpretation by Batulzii, Holk and Bayartsengel).

Texture of granite outcrops of distinguished intrusions, their relationships, dikes, roof pendant and mineralization: The interpreted intrusions differ primarily in the texture of their outcrops. Enhanced weathering along intersecting joints imparted a spheroidal surface appearance for intrusion I-W. This arcuate-shaped, I-W intrusion is mostly composed of coarse-grained, porphyritic and agpaitic aegirine-arfvedsonite granites. Outcrops of II-W are characterized by vertical joints that were intersected by shallow-dipping, closer-spaced joints. Intrusion II-W is represented by pale pink, medium-to-coarse-grained, equigranular and porphyritic, aegirine-arfvedsonite granites. The content of elpidite in some places exceeds the content of accessory minerals. The outer contact zone II-W is not only controlled by the uplifted host rocks but also by banded pegmatite zones with quartz cores. Rough, fractured surfaces characterize the outcrops III-W. Primarily, structures were destroyed by dikes from IV-W. The outcrop of this intrusion was documented by Kovalenko et al., but the compositional character has not been studied [19]. Contrasting colors and textural shapes define the intrusive contact between units II-W and III-W. The contact where III-M intrudes II-M is visible by their colors and shapes. The intrusion III-M is composed of brown-reddish medium-grained aegirine-arfvedsonite granites. Intrusion IV-M is distinguished from others by their red color and outcrop shape formed by intersecting vertical and horizontal sets of joints. These red porphyritic granites have plagioclase phenocrysts, along K-feldspar and ferro-edinite (Figure 3).

As mentioned above, two intrusions comprise the Eastern body. Scattered roof pendants indicated by a blackish color in the landsat images occur among the red granites of II-E.

Apophyses of II-E into I-E and I-W demonstrate its younger origin. Granites II-E are characterized by aegirine and red K-feldspar phenocrysts embedded in a fine-grained reddish groundmass. The older I-E is characterized by medium-grained spherical-textured lilac granites, where pinkish K-feldspar phenocrysts are in a lilac groundmass (Figure 4).

Figure 3: Outcrop and hand specimen photos of alkali granites in the Western body of Khanbogd pluton. **Note:** (a) outcrop of intrusion I-W; (b) coarse-grained porphyritic texture greyish color aegirine-arfvedsonite granite in intrusions I-W; (c) outcrop of II-W, where dominated horizontal platy joint; (d) elpidite rich agpaitic, greyish color granite in intrusion II-W; (e) outcrop of III-W, intruded into II-W; (f) reddish color aegirine-arfvedsonite granite in III-W; (g) outcrop of IV-W, where cubic shape is formed from set of vertical and horizontal joints; (h) red color, ferro-edinite granite.

Figure 4: Outcrop and hand specimen photos of alkali granites in the Eastern body and outcrop of dike and pegmatites. **Note:** (a) host rock roof pendants among red granite intrusion I-E; (b) relationship between I-E and II-E: granite II-E intrude into I-E; (c) hand specimen of the porphyry texture red granite; (d) hand specimen of lilac granite; (e) comendite dike outcrop intruding III-W granite; (f) pantellerite lava lying in granite II-M; (g) ekerite composition sheet pegmatites in intrusion I-M; (h) outcrop of andesite roof pendant.

Dikes of various compositions have been identified in the Khanbogd pluton. Thus, in the arcuate intrusion, there are subparallel dikes of ekerites and pegmatites with arfvedsonite and elpidite. Red comendite dikes with large K-feldspar phenocrysts are common in granites II-W. Dark gray pantellerite dikes and elpidite-bearing smaller pegmatites are described from intrusions II-W and III-W.

However, Mongolian researcher Garamjav offered, that a shape-like ring of the Khanbogd pluton must be associated with the rise of magma in the form of a vortex. The primary structure study of the granites does not show a foliation structure, which has to follow a vortex event. The foliation is defined from some pegmatites and dikes [44,45].

The trachydacite in the roof pendant has a Carboniferous age of 330 Ma, that is dark brown in Landsat images. Following identifying several intrusions, we revise the location of REE mineralization. The horizontal pegmatites, consisting predominantly of large crystals of arfvedsonite-elpidites, occur in the southern part of the arc-shaped I-W intrusion. Zirconium and niobium oxides such as pyrochlore, monazite, armstrongite, mongolite and gittincite were described from pegmatites that are in II-W.

Oxygen and hydrogen isotope study

Oxygen isotope values from coexisting quartz, K-feldspar and arfvedsonite and δ D values of arfvedsonite from Khanbogd granite intrusions are indicated in Supplementary Table 1. The mineral $\delta^{18}O$ values are compared to test for equilibrium to assess magma sources. Arfvedsonite dD values were used to determine whether granites were affected by the hydrous process.

The quartz and K-feldspar $\delta^{18}O$ values are out of equilibrium with the feldspars being shifted to lower values. This indicates oxygen isotope exchange between a meteoric-hydrothermal fluid and feldspar [46].

The disequilibrium occurs because feldspar group minerals exchange oxygen much faster than quartz. Many of the quartz $\delta^{18}O$ values cluster between 8 and 9.5 per mil. This narrows down the oxygen isotopic composition of the primary magma. The meteoric fluid system was short-lived because if it had been active over a longer period, the quartz would have been shifted to a lower $\delta^{18}O$ value to be in equilibrium with the feldspar at a lower value [47].

However, some quartz $\delta^{18}O$ values have also been shifted downward. These are common characteristics of intrusions emplaced into the shallow crust.

Few samples in the equilibrium field including granites II-E show the $^{18}O/^{16}O$ isotope ratios of quartz were changed to a lesser extent, more likely. Exceptionally, $\delta^{18}O$ low values of quartz and K-feldspar are found in granites I-E and dikes (Figure 5).

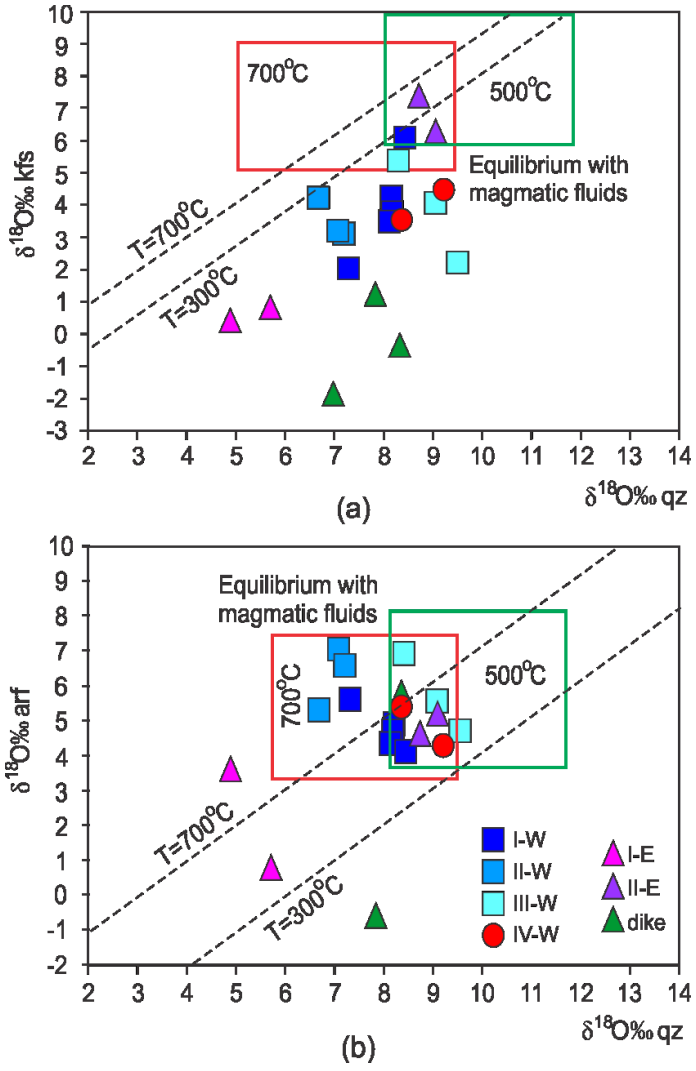

Figure 5: Equilibrium fields of quartz and K-feldspar fractionation in (a) is from Zheng et al., (b) is from Zheng et al., Minerals abbreviation.
Note: (a) plots in $\delta^{18}O\%$ qz– $\delta^{18}O\%$ kfs diagram, (b) plots in $\delta^{18}O\%$ qz– $\delta^{18}O\%$ arf diagram.

In addition, the real low dD values (-201 to -156) from arfvedsonite and ferro-edenite support the argument for the involvement of meteoric-hydrothermal fluids [22-26]. In the δ^{18} Oqz *vs* δ^{18}O arf diagram, data for these minerals of all granites are plotted in an equilibrium field, except I-E and the dike data [45]. Across it, the data of some granites, particularly granites II-W, are plotted in the equilibrium field of T 700°C. Most granites are grouped in areas where the equilibrium T0 is between 700-5000C. According to Taylor [46], anatectic melting producing the formation of peraluminous leucogranite magmas must have occurred after a hydrothermal event that homogenized the $^{18}O/^{16}O$ and $^{87}Sr/^{86}Sr$ ratios of pelitic metasediments.

Therefore, the δ^{18}O values of arfvedsonite were equilibrated with the magmatic δ^{18}O values of quartz, although the dD values are much lower.

Water contents from arfvedsonite and ferro-edenite are generally low (<2.0%), however, an arfvedsonite of a comendite dike contains 7.4% H_2O (Supplementary Table 1). An elpidite from a pegmatite has δD = ¬–87% and an H_2O content of 8.3%, suggesting alteration by magmatic fluids (Supplementary Table 1).

Petrographical studies of the alkali granites

The alkali granites contain 65%-70% microcline, 25%-28% quartz and a lesser amount of albite (3%-5%), arfvedsonite and aegirine or ferro-edenite (3%-9%). Garnet is less than 2.0% in granites. Agpaite texture is common for studied granites. This study describes a domain structure indicative of a time gap caused by cold meteoric water accompanying nonequilibrium crystallization. The structure such as lobate, convolute and dislocation boundaries at the contact of K-feldspar and quartz were discussed as a domain structure by Joekar-Niasar, et al., Effects similar to such structures were considered as the result of changes in the $^{18}O/^{16}O$ ratio in K-feldspar and quartz by Holk and Tayle.

The contact between quartz and K-feldspar is different, sometimes direct and some are convolute and lobate (Figure 6). The fractured and stippled surfaces in the microcline are akin to the effects of oxygen isotope changes. Albite growth effects are observed in potassium feldspar. In the upper part of the photo, albite growth looks like drops and they are dense. Below, the drops are mixed with tabular albites and further on, needle-like intergrowths of albite are observed in K-feldspar. The dislocated boundaries between K-feldspar and quartz, new crystals along fracture zones in K-feldspar, are explained by effects associated with isotopic changes. Aegirine crystals occur between quartz and K-feldspar; less common, aegirine is grouped with either garnet or arfvedsonite. A changed surface in K-feldspar and a dislocated boundary at the contact of aegirine and K-feldspar are noted.

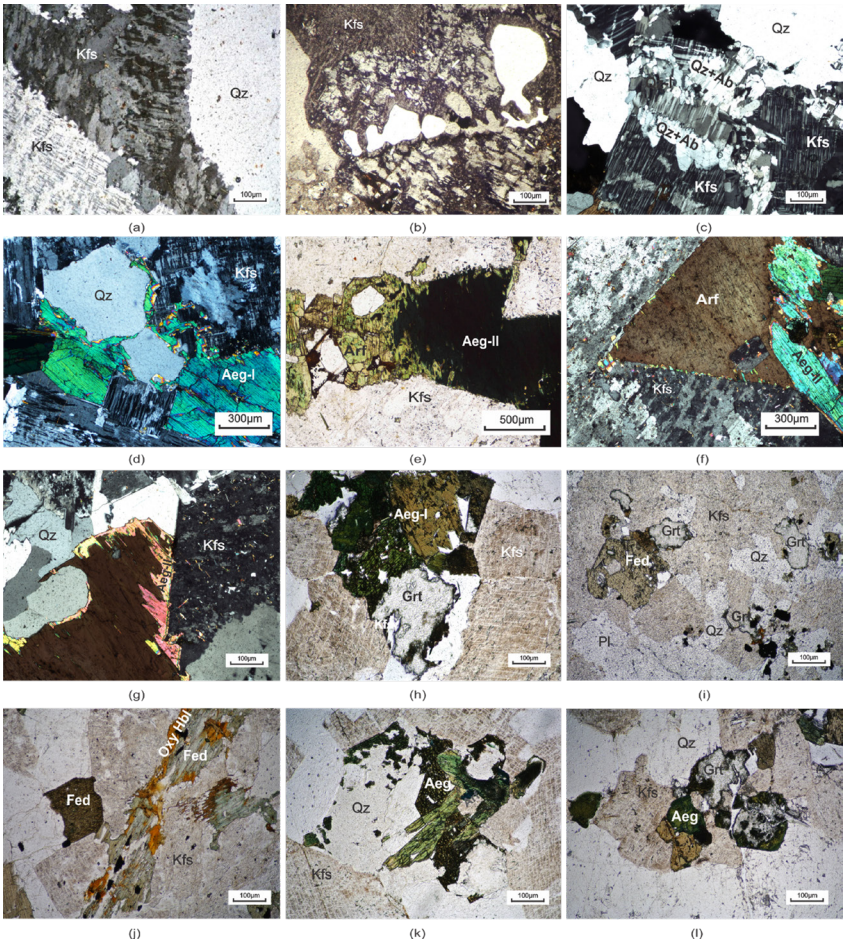

Figure 6: Petrographical studies of the alkali granites **Note:** (a) Lobate boundary between quartz (Qz) and fractured K-feldspar (Kfs); (b) convolute boundary between quartz and K-feldspar with albite growth; (c) dislocated boundary with new quartz along a fracture zone; (d) dislocated/lobate boundaries between aegirine, K-feldspar and quartz; (e) lobate boundary from arfvedsonite to I-stage aegirine; (f) domain boundary of arfvedsonite and aegirine in K-feldspar; (g) stage-II aegirine into arfvedsonite; (h) garnet corroded by aegirine; (i) ferro-edinite with relict garnets; (j) oxy-hornblende replacing ferro-edinite; (k) aegirine replaced by arfvedsonite; (l) garnet corroded by aegirine. Non-crossed nicol: b, e, h, i, j, k, l.

Between aegirine K-feldspar and aegirine arfvedsonite, convolute and lobate boundaries are often found, indicating a domain structure. Similar boundaries are observed in contact with potassium feldspar and aegirine, the latter being considered a peritectic phase mineral of alkali granites. Wedge-shaped aegirine crosses the arfvedsonite and K-feldspar contact and the lobes around arfvedsonite were filled with aegirine plates. Thus, two-stage aegirine crystals are distinguished and differ in time, both before and after arfvedsonite. The thin needles and drops of arfvedsonite and aegirine-II in K-feldspar represent the diffusion domain. The stage-I aegirine is always associated with garnets in I-W, II-W and III-W granites. Garnets are easily marked in thin sections from III-W, corroded by aegirine.

The amphibole of granite IV-M refers to the ferro-edenite [47]. Granite composed by the microcline 60%-62%, quartz 25%-27%, plagioclase 9%-12%, ferro-edenite 2%-4%, approximately. This granite also contains garnets of various sizes. The droplets of ferro-edenite in K-feldspar IV-M granites represent the domain structure. There is also brown oxygen-hornblende replacing the ferro-edinite.

The granites of the Eastern body are predominantly fine-grained, the amount of ferrous minerals is 2%-4% in the volume of granites. The fibrous and stellate form aegirine is characteristic of granites I-E. Arfvedsonite, which selectively replaces aegirine, is dark bluish compared to arfvedsonite in the granites of the Western body. The garnet with size from 0.03 × 0.01 mm is more conspicuous for granites II-E. A distinctive feature of these granites is absence of stage-II aegirine.

Geochemistry of the Khanbogd alkali granites

Chemical analysis of oxides and calculated CIPW norms of the granites are listed in Supplementary Table 2. Regardless of the presence of ferro-edenite, all granites in the TAS and AQPF diagrams are represented by alkali granites. The granites of all interpreted intrusions differ in their aluminum saturation index (ASI) e.g., [48,49]. Accordingly, granites of I-W, II-W and I-E intrusions are peralkaline. Granites III-W shows peraluminous affinity; the granites II-E vary from metaluminous to peraluminous. Identical affinity for them is co-crystallized aegirine and arfvedsonite, as well as the amount of garnet. Hence, ferro-edenite granites are plotted in the metaluminous granite field excluding one. Figures 7b- 7f show a correlation between oxides and differentiation index (D.I) e.g., [50]. The silica content in granites of all intrusions is 71.00%-78.36%. The granites of the Eastern body are characterized by a high DI and differ from the granites of the Western body. Ferro-edinite granites are distinguished by SiO_2, CaO, MgO and K_2O content from aegirine-arfvedsonite granites (Supplementary Table 2, Figures 7b-7f). FeOt variations indicate that the aegirine-arfvedsonite content in the granites of the Eastern body is less than in the granites of the Western body. Accordingly, they (I-E and II-E) are characterized by low Na_2O, K_2O and FeOt content compared to the Western body's granites. The studied granites also differ well in their CIPW norm calculated using the Hollocher program [51]. Granites I-M and II-M are acmite-Na-silicate (acm-ns) normative, except for a small amount of ferrosilite (fs) and enstatite (en) molecules. Ilmenite is in norm from these granites. The anorthite- hypersthene (an-hyp) molecule is calculated from aegirine-arfvedsonite granite III-M. The an-hyp-di norm is acquired from ferro-edenite granites. Only acmite is calculated from granites I-E, which is peralkaline and an-hyp±di norm is calculated from II-E, which exhibit a metaluminous-peraluminous character. The norm of ilmenite (il) of the I-W and II-W granites implies that they derived from a more reduced environment than others, for which a near-neutral condition predominated. According to the K_2O/Na_2O ratio, all granites are rich in potassium; ekerite and pantellerite dikes are rich in Na and characterized by the acmite, Na-silicate and ilmenite norms. Comendites are potassium-rich and exhibit acmite or anorthite norm (Supplementary Table 2) (Figure 7) [52-56].

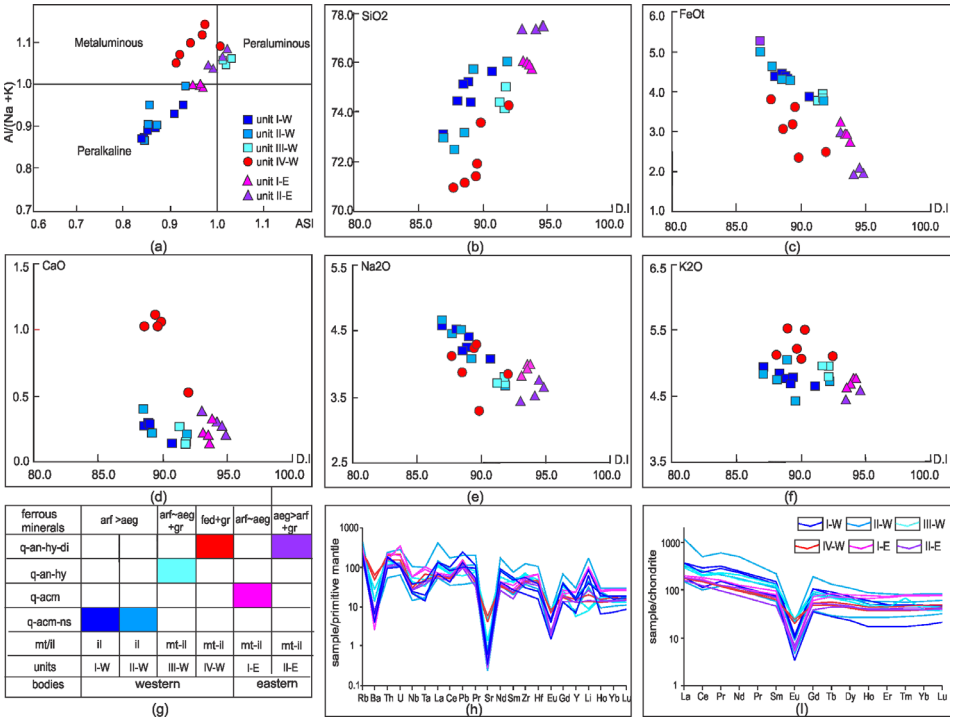

Figure 7: Correlation diagrams **Note:** (a) Granite plots in the ASI diagram; (b-f) oxide *vs* differentiation index (D.I) plots; (g) calculated norms from alkali granites across different intrusions; (h) primitive mantle-normalized multi-element patterns of alkali granites; (i) chondrite-normalized REE patterns of alkali granites from various intrusions, with normalized values from Sun and McDonough; I-W (■); II-W(■); III-W(□); IV-W (●);I-E(▲); II-E(▲).

The trace and REE analysis of the granites are shown in Supplementary Table 3. The Li content is 31.75 ppm-71.02 ppm for granites I-W and 5.85 ppm-14.97 ppm for granites IV-W. Some samples contain high Zr content having zirconium oxides such as elpidite (Supplementary Table 3). In the trace element distribution diagram normalized to the primitive mantle, deep negative anomalies of Ba, Sr and Eu and positive anomalies of Th, U, Pb and Li are observed. The largest negative anomalies of Ba and Sr are detected in all patterns. Although, less pronounced negative anomalies of Ba, Sr and Eu are marked from ferro-edenite granites. The chondrite normalized REE patterns from granites are sub-symmetric, with Eu deep negative anomalies. In this diagram, the patterns of the ferro-edenite granites are intermediate between those of the others and the Eu anomalies are at a higher level than the others.

The geochemistry of studied alkaline granites with low Sr, Ba, Eu, Ti and high Th, U and Pb contents resembles the vapor-absent melt crystallization from the High-Himalayan Mountains.

Sr, Nd, Hf, Pb, O and H isotopes of the alkali granites Khanbogd pluton

The initial $^{87}Sr/^{86}Sr$ and 143Nd/144Nd were calculated for samples on Rb-Sr whole rock isochron age of 295.7 Ma and the Sr isotope ratios were measured for most samples. The 295.7 Ma was obtained twice, first from all aegirine-arfvedsonite granites, including ekerite and comendite dikes and second from granites I-M, II-M and III-M (Supplementary Table 4). According to this measurement, $^{87}Sr/^{86}Sri$ values range from 0.6676 to 0.7077 for the aegirine-arfvedsonite granites, except for one value of 0.7287.143Nd/144Ndi values of the granites are moderately high, from 0.5125 to 0.5127. A slightly higher initial $^{87}Sr/^{86}Sr$ of 0.7051-0.7071 was obtained from ferro-edenite granites with their isolated plots of 269.6 ± 2.8 Ma (Supplementary Table 5). Also, 291 ± 7.2 Ma was detected from aegirine-arfvedsonite granites of two bodies, excluding dikes, (Supplementary Table 4). The received ages of 291 ± 7.2 and 295.7 ± 5.3 Ma are consistent with U/Pb zircon dating by Kovalenko et al., [19]. These are 290 ± 1 Ma for coarse-grained granite and 292 ± 1 Ma for a pegmatite I-M. The latest U/Pb ages of zircons were obtained from granites of the Eastern body during the prospecting project on U and REE. The studied site occupied the southern half of the Eastern body. Zircon U-Pb ages were analyzed at the Shandong testing center of China Metallurgical Geology Bureau in Jinan city of Shandong province, China. Samples were taken from drill cores. Obtained concordia ages are 287 ± 3.6 Ma, 288 ± 3.0 Ma and 289 ± 3.6 Ma.

All εNdt values are positive in the range 5.82-7.80 for aegirine-arfvedsonite granites, 3.95-5.99 for ferro-edenite granites and 5.06-6.97 for dikes, (Supplementary Table 5). Isotopic plots in the $^{87}Sr/^{86}Sri$-$^{143}Nd/^{144}Ndi$; $^{207}Pb/^{204}Pb$-$^{206}Pb/^{204}Pb$; εNd(t)-εHf(t) and Sri-$\delta^{18}O$% diagrams indicate that modified oceanic rocks were involved in the melting source of alkaline granites (Figure 8).

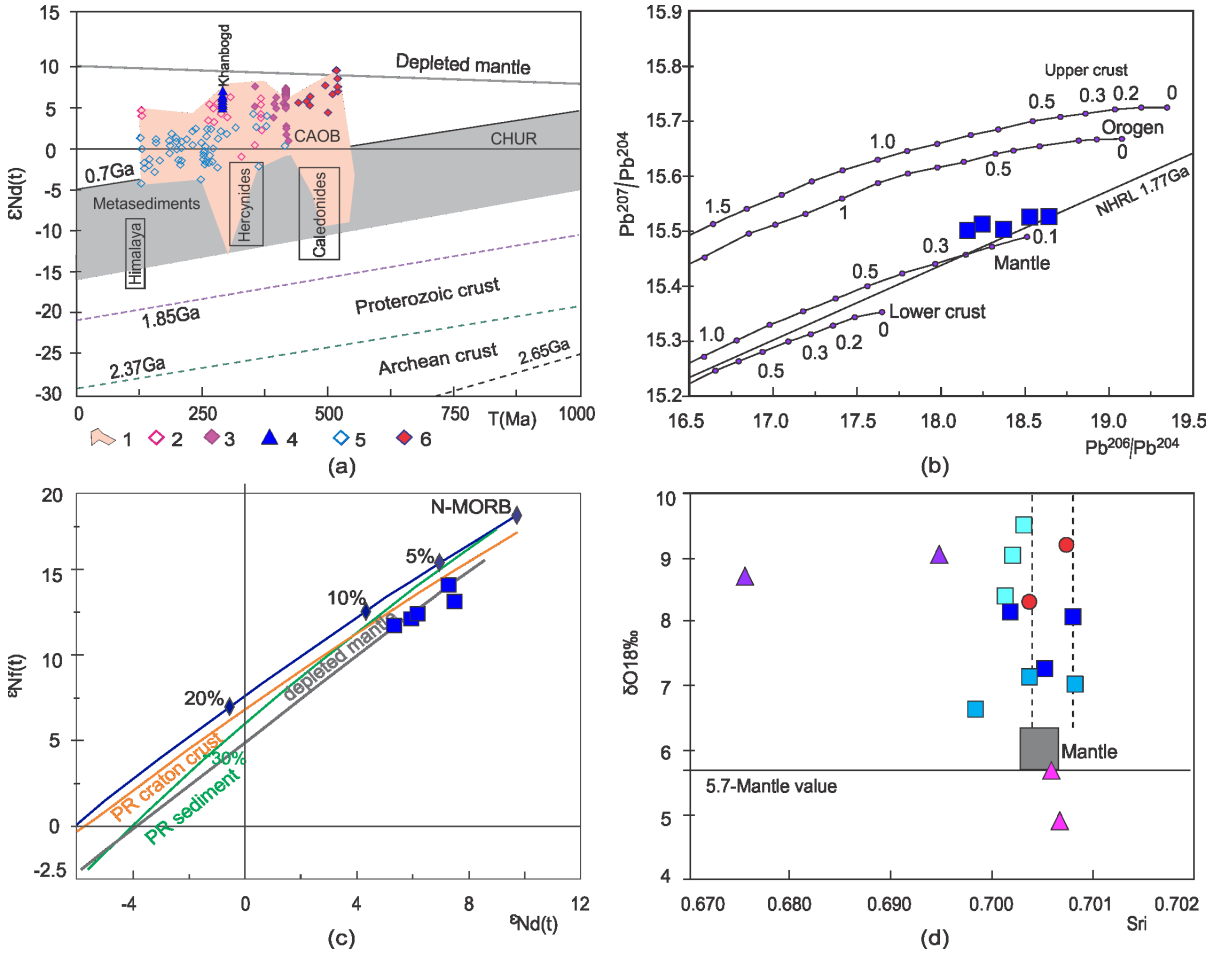

Figure 8: Isotope data plots from Serjlkhumbe. **Note:** (a) Plots in $^{87}Sr/^{86}Sri$ *vs* 143Nd/144Ndi diagram; (b) plots in Pb isotopic systematics upper and lower crust, orogen and mantle evolution curve by, Tick marks represent 0.1 Ga age intervals; (c) plots in εHf (t) *vs* εNd(t) diagram, N-MORB, Proterozoic continental crust, Proterozoic sediment data and mantle arrow are from; (d) data plots in $^{87}Sr/^{86}Sr$ - $\delta^{18}Oqz$ diagram, modified from Magaritz et al., The dotted lines are approximate ranges of $^{87}Sr/^{86}Sri$ - $\delta^{18}Oqz$ in mantle-derived rocks.

Results and Discussion

Fault zones controlled by uplifted country rocks indicate the emplacement of laccoliths, sills, sheets and ring dikes in response to magma injection along faulted country rocks or bedding in host rocks. This resulted in the Khanbogd pluton and identified several horizontal elliptical intrusions within the pluton. Our model for these alkali granites invokes magma underplating of duplex-type thrusts, consistent with the model of Konstantinovskaya and Malavielle. Evidence includes two adjacent intrusive bodies and undeformed Carboniferous volcanic rocks at the front of the pluton [57-60].

Geology and Petrogenesis

Fault zones controlled by uplifted country rocks indicate the emplacement of laccoliths, sills, sheets and ring dikes in response to magma injection along faulted country rocks or bedding in host rocks. This resulted in the Khanbogd pluton and identified several horizontal elliptical intrusions within the pluton. Our model for these alkali granites invokes magma underplating of duplex-type thrusts, consistent with the model of Konstantinovskaya and Malavielle. Evidence includes two adjacent intrusive bodies and undeformed Carboniferous volcanic rocks at the front of the pluton.

The studied granites exhibit a variety of phenomena associated with meteoritic fluids. Much lower δD values of arfvedsonite (-141% to -171%) indicate the involvement of high-latitude meteoric-hydrothermal fluids [27]. These lowest dD values are also consistent with Late Paleozoic glaciation, noted in both hemispheres, in the Early Permian and Triassic timer e.g. [61].

The agpaite texture in studied granites indicates that quartz and K-feldspars crystallized first from the solid phase melt when the temperature reached their crystallization T0C. Accordingly, the residual solid phase was enriched with Mg-Fe components. A peritectic phase from vapor absent melt has been proposed for alkali pyroxene by the experimental data of Patino Douce. Garnet is a co-crystalized mineral with pyroxene in that experiment. This shows they may form from the peritectoid-like system, where two solid phases are suggested from the decomposing of the solid phase. The dominant aegirine crystals show, that pertictoid system transformed into a peritectic phase and continued aegirine crystallization. We intend that arfvedsonite can form from modified or initiated by the meteoric fluids peritectic phase. Most likely, the intersection of aegirine and arfvedsonite crystals indicates that the reaction producing aegirine has changed from an anhydrous to a hydrous state and formed arfvedsonite. The structures of aegirine and arfvedsonite, inferred from the peritectic and lagging phases, are similar. This may be due to the time gap that occurred in both cases. Crystals and droplets of stage-II aegirine may be associated with the diffusion of magnetization change from the hydrous to the anhydrous state in the crystallization source.

Further, meteoric hydrothermal fluids resulted in disequilibrium $\delta^{18}O$ values between quartz and feldspar, which occurred in the post-solidus state [44]. Hydrothermal fluid was short-lived (<100ka), as evidenced by the faster exchanging feldspars having experienced a greater degree of $^{18}O/^{16}O$ exchange than co-existing quartz e.g., [62]. In addition, the effects in K-feldspar crystals are consistent with changes evidenced by hydrothermal fluids.

The vapor absent melt crystallization in granitoid from emplacement in thrust sense shear zones has been described since early e.g., [63,64]. The geochemistry characteristic of studied alkaline granites with low Sr, Ba, Eu, Ti and high Th, U and Pb is consistent with this crystallization.

Magma source of the Khanbogd alkali pluton and gravimetric model of another alkali-granite Bayan-Ulaan pluton

The $^{87}Sr/^{86}Sr$-$\delta^{18}O$ correlation diagram illustrates the sources: i) seafloor sediments, ii) depleted mantle and iii) Precambrian gneisses and paleozoic rock. Ocean-floor sediments are considered a resource of Rare Earth Elements e.g [65-68]. Therefore, the REE concentration in the alkaline granites of Khanbogd pluton does not negate the participation of modified ocean floor rocks in their magmatic source. The $^{87}Sr/^{86}Sri$ and $^{18}O/^{16}O$ ratios of studied granites are mainly suitable for the depleted mantle and source derived from the lower continental crust (Supplementary Table 4). Also, identical to the ratios of amphibolite and granulite [69]. The tonalites and granodiorite compositions studied by Blight e.g., [70] in southern Mongolian from Early Carboniferous arcs. These rocks and the rocks that produce them may be the melt source of the Khanbogd alkaline granite (Figure 9).

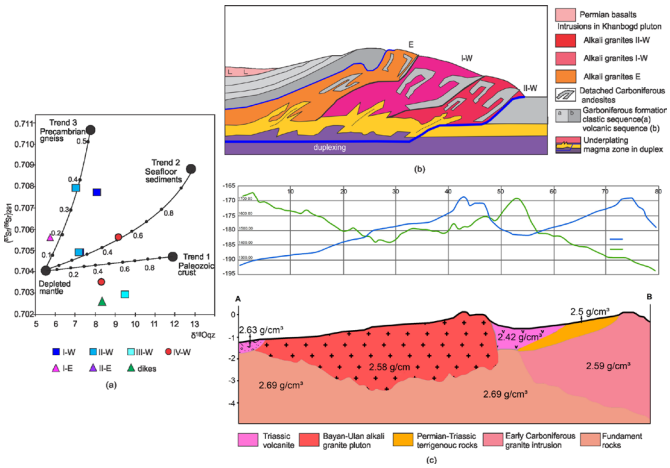

Figure 9: Model for Khanbogd pluton. **Note:** A-plots in $^{87}Sr/^{86}Sr291$ - $\delta^{18}Oqz$ diagram. Trend curves of terrigenous sediment from, seafloor sediment from and depleted mantle from Eiler et al.

The much lower sri values of 0.6087-0.6089 were obtained from granite II-E intrusion. It was the last intrusion in the pluton. There is a small site with Mo mineralization on the southern margin of I-M intrusion, which has contacted II-E in its continuous. Therefore, the sri values 0.6087-0.6089 of intrusion II-E imply those changes by the ore-bearing hydrothermal fluids. Figure 9b presents our model for the studied Khanbogd pluton. The latest U/Pb ages from the Eastern body within 287-289±3.6 Ma are consistent with its formation later than the Western body [52].

A gravimetric model of another largest alkali-granite pluton, Bayan-Ulan, located in Central Mongolia, was done by geophysicists of the "Geo-Oron" company. As a result of modeling, a flattened shape was obtained for this pluton [71-74]. The Bayan-Ulan pluton occupies almost 1000 sq. km and is emplaced into an accretionary wedge complex. The underplate magma model has mainly been proposed for anorogenic igneous rocks of the rifting e.g [73-76]. According to Stel et al., this magmatic event is also observed in basins where crustal extension did not occur. The detrital zircon age of this complex correlated to the interval of Permian-Triassic [73,77-80]. The granites of the Bayan-Ulan pluton consist predominantly of quartz, K-feldspar and aegirine, with a minority of riebeckite and biotite. The U/Pb zircon age of 221 Ma was determined from alkaline granite [81-84]. The leucogranite is associated with alkali granites

in this pluton. The measured dD values from riebeckite are in (-181) - (-210%) [85]. The δ^{18}Oqz values ranged from -9.94% to -7.56% and δ^{18}Okfs values from -0.06% to-8.53% are shown those mineral's disequilibrium [86-88].

Similar events, such as magma rising along horizontal faults and underplating magma sources, were suggested for the Permian alkaline granite plutons of China. This shows that the Permian alkali granite plutons were evidenced by similar processes, maybe by rifting in southern Mongolia and northern China [89].

Conclusion

The peralkaline Khanbogd plutonic complex, with an area over > 1000 sq. km, was formed by the sequential emplacement of several elliptic intrusions along the sub-horizontal fracture zones from duplex-type thrusting. The co-crystallization of aegirine and arfvedsonite or only arfvedsonites in alkali granites, shows the presence of hydrothermal fluid at their formation. The disequilibrium of δ^{18}O values between quartz and feldspar caused by meteoric fluids is expressed by effects at their boundaries and the surface. These effects such as convolute, lobate and stippled surfaces are similar to the domain structure of arfvedsonite that resulted during the crystallization process. The intersection of aegirine and arfvedsonite crystals led us to conclude that the arfvedsonite could have formed from a changed peritectic phase producing aegirine. The convolute, lobate boundaries of aegirine and arfvedsonite imply that a time gap occurred in the initiation of both phases. Droplets, considered domains are formed from an opposition water-exhausted state, due to magnetization changes. The higher alkalinity associated with low Sr, Nd, Hf and Pb isotopes of alkali granites indicates their formation from an underplate melt during duplex thrust, where oceanic and mantle-sourced rocks were involved.

Funding

Field geological studies of this large pluton were re-examined as part of the project “Accretional Orogen of Southern Mongolia: A Comparison of the Central Asian Orogen (CAOB) in Mongolia and China - (NFSC2019/04). The geochemical analyses were carried out by Dr. Amaramgalan’s master's and doctoral thesis, provided by the Monbusho grant of the Japanese Ministry of Education and Culture.

Acknowledgments

We must thank our previous scientists, such as Vladykin. N.V. and Kovalenko. V.I. and others, who devoted many years of their work and life to the study of this pluton. Our great thanks to Professor Ochir Gerel who requested to study alkaline granites Khanbogd pluton. We also thank Professor Thomas K. Kelty for initiating our collaborative work with California State University Long Beach (CSULB) where the oxygen isotope analysis was conducted. A respected friend and colleague of many scientists and geologists, Prof. Yin An, remains in our memory, but his contribution to this manuscript is invaluable. Blessed memory to him. We specially thanked young geologists Tseveendorj Bayartsengel, Baatar Gendenjamts, Ganbat Turbat, Byambajav Tankhildulam, Dembee Unurzaya and director Ulamsain, Ya of “Geo-Oron” LLC and geologist of “Magnetic survey” LLC who cooperated and helped to develop this manuscript.

References

1. Jahn BM, Wu F, Chen B (2000) Granitoids of the Central Asian Orogenic Belt and continental growth in the Phanerozoic. Earth Envi Sci Trans Royal Soci Edinburgh 91(1-2):181-93.
2. Eby GN (1990) The A-type granitoids: A review of their occurrence and chemical characteristics and speculations on their petrogenesis. Lithos 26(1-2):115-34.
3. Foland KA, Allen JC (1991) Magma sources for Mesozoic anorogenic granites of the white mountain magma series, New England, USA. Contrib Mineral Petrol 109(2):195-211.
4. Han BF, Wang SG, Jahn BM, Hong DW, Kagami H, Sun YL (1997) Depleted-mantle source for the Ulungur River A-type granites from North Xinjiang, China: Geochemistry and Nd–Sr isotopic evidence and implications for Phanerozoic crustal growth. Chemical Geolog 138(3-4):135-59.
5. Loiselle MC (1979) Characteristics and origin of anorogenic granites. Geol Soc Am 11:468.
6. Collins WJ, Beams SD, White AJ, Chappell BW (1982) Nature and origin of A-type granites with particular reference to southeastern Australia. Contrib Mineral Petrol 80:189-200.
7. Creaser RA, Price RC, Wormald RJ (1991) A-type granites revisited: Assessment of a residual-source model. Geology 19(2):163-6.
8. Harris NB, Marriner GF (1980) Geochemistry and petrogenesis of a peralkaline granite complex from the midian mountains, Saudi Arabia. Lithos 13(4):325-37.
9. Patino Douce AE (2005) Vapor-absent melting of tonalite at 15–32 kbar. J Petrol 46(2):275-90.
10. Skjerlie KP, Johnston AD (1992) Vapor-absent melting at 10 kbar of a biotite-and amphibole-bearing tonalitic gneiss: Implications for the generation of A-type granites. Geology 20(3):263-6.
11. Bailey DK (1987) Mantle metasomatism—perspective and prospect. Geol Society 30(1):1-3.
12. Currie KL, Eby GN, Gittins J (1986) The petrology of the Mont Saint Hilaire complex, southern Quebec: An alkaline gabbro-peralkaline syenite association. Lithos 19(1):65-81.
13. Whitney DL, Evans BW (2010) Abbreviations for names of rock-forming minerals. American mineralogist. 95(1):185-7.
14. Dostal J, Owen JV, Gerel O, Keppie JD, Corney R, et al. The 186 Ma Dashibalbar alkaline granitoid pluton in the North-Gobi rift of Central Mongolia: Evidence for melting of Neoproterozoic basement above a plume. Amer J Sci 314(2):613-48.
15. Dostal J, Owen JV, Shellnutt JG, Keppie JD, Gerel O, et al. (2015) Petrogenesis of the Triassic Bayan-Ulan alkaline granitic pluton in the North Gobi rift of central Mongolia: Implications for the evolution of Early Mesozoic granitoid magmatism in the Central Asian Orogenic Belt. J Asian Earth Sci 109:50-62.
16. Bonin B (1998) Alkaline rocks and geodynamics. Turkish J Earth Sci.7(3):105-18.
17. Vladikin NB, Kovalenko VI, Dorfman MD (1981) Mineralogical and geochemical characteristics of Khanbogd peralkaline granite pluton: Moscow, Nauka.
18. Kovalenko VI, Yarmolyuk VV, Kozlovsky AM, Kovach VP, Sal’nikova EB, et al. (2007) Two types of magma sources of rare-metal alkali granites. Geology of Ore Deposits 49:442-66.
19. Kovalenko VI, Yarmoluyk VV, Sal’nikova EB, Kozlovsky AM, Kotov AB, et al. (200) Geology, geochronology and geodynamics of the Khan Bogd alkali granite pluton in southern Mongolia. Geotectonics. 40:450-66.
20. Serjlkhumbe A (2008) U-Pb geochronology and multi-isotopic systematics of granitoids from Mongolia, central Asian orogenic belt: Implications for granitoid origin and crustal growth during the Phanerozoic.
21. Serjlkhumbe A (2004) Petrological and geochemical studies on the Khanbogd alkaline complex, South Mongolia.
22. Nowell GM, Kempton PD, Noble SR, Fitton JG, Saunders AD, et al. (1990) High precision Hf isotope measurements of MORB and OIB by thermal ionisation mass spectrometry: Insights into the depleted mantle. Chem Geol 149(3-4):211-33.
23. Sharp ZD, Atudorei V, Durakiewicz T (2001) A rapid method for determination of hydrogen and oxygen isotope ratios from water and hydrous minerals. Chem geol 178(1-4):197-210.
24. Sharp ZD (1990) A laser-based microanalytical method for the in situ determination of oxygen isotope ratios of silicates and oxides. Geochim Cosmochim Acta 54(5):1353-7.

25. Sheppard SM (1986) Characterization and isotopic variations in natural waters. Rev Mineral Geochem 16(1):165-83.
26. Sheppard SM, Brown PE, Chambers AD (1977) The Lilloise intrusion, East Greenland: Hydrogen isotope evidence for the efflux of magmatic water into the contact metamorphic aureole. Contrib Mineral Petrol 63(2):129-47.
27. Taylor Jr HP, Forester RW (1979) An oxygen and hydrogen isotope study of the Skaergaard intrusion and its country rocks: A description of a 55 my old fossil hydrothermal system. J Petrol20(3):355-419.
28. Zheng YF (1993) Calculation of oxygen isotope fractionation in hydroxyl-bearing silicates. Earth Planet Sci Lett 120 (3-4):247-63.
29. Taylor (1988) Oxygen, hydrogen and strontium isotope constraints on the origin of granites. Earth Env Sci 79, 317-338.
30. Thouret JC, Finizola A, Fornari M, Legeley-PA, Suni J, et al. (2001) Geology of El Misti volcano near the city of Arequipa, Peru. GSA Bulletin 113(12):1593-610.
31. Liu W, Zhao Z, Zhang, F(1999)Oxygen and hydrogen isotopic compositions of coexistent minerals of the Tasigake alkali granite pluton, northern Xinjiang: Constraints upon the cause of 18O-D depletion and the $^{18}O/^{16}O$ exchange kinetics. Chinese Science Bulletin 44, 1086–1093.
32. Joekar NV, Hassanizadeh SM, Dahle HK (2010) Non-equilibrium effects in capillarity and interfacial area in two-phase flow: Dynamic pore-network modelling. J Fluid Mech 655:38-71.
33. Gröning M (2004) International stable isotope reference materials. Stable isot analyt tech.
34. Taylor Jr HP, Epstein S (1962) Oxygen isotope studies on the origin of tektites. J Geophys Res 67(11):4485-90.
35. Kimura J (1995) Igneous rock analysis using ICP-MS with internal standardization, isobaric ion overlap correction and standard addition methods. Sci Rep Fukushuma Univ 1995;56.
36. Iizumi S (1996) Sr and Nd isotope analyses, using a thermal ionization mass spectrometer MAT262. Geosci Rep Shimane Uni 15:153-9.
37. Iizumi S, Maehara K, Morris PA, Sawada Y (1994) Sr isotope data of some GSJ rock reference samples. Mem Fac Sci Shimane Univ 28:83-6.
38. Vladykin N, Drits V, Kovalenko V, Dorfman M, Malov V, et al (1985) Novyj sikokiat-niobiya-mongolit Ca_4Nb_6 (Si_5O_20) O4 (OH10) nH_2O. Zapiski Vsesoûznogo mineralogičeskogo obŝestva. 1985(3):374-5.
39. Vladykin Nv, Kovalenk. Vi, Kashaev Aa, Sapozhni. An, Pisarska. Va (1973) New silicate of calcium and circonium-armstrongite. Doklady Akademii Nauk Sssr 209(5):1185-8.
40. Kynicky J, Chakhmouradian AR, Xu C, Krmicek L, Galiova M (2011) Distribution and evolution of zirconium mineralization in peralkaline granites and associated pegmatites of the Khan Bogd complex, southern Mongolia. Can Miner 49(4):947-965.
41. Kozlovsky AM, Yarmolyuk VV, Kovalenko VI, Savatenkov VM, Velivetskaya TA (2007) Trachytes, comendites and pantellerites of the Late Paleozoic bimodal rift association of the Noen and Tost ranges, southern Mongolia: Differentiation and contamination of peralkaline salic melts. Petrology 15:240-263.
42. Kozlovsky AM, Yarmolyuk VV, Sal'nikova EB, Savatenkov VM, Kovalenko VI (2005) Age of Bimodal and Alkali Granite Magmatism of the Gobi–Tien Shan Rift Zone, Tost Range, Southern Mongolia. Petrologiya 13(2):218-224.
43. Yanshin LA (1989) Geological formations map of Mongolian People's Republic, scale 1: 1500000.
44. Yarmolyuk VV, Kovalenko VI, Sal'Nikova EB, Kovach VP, Kozlovsky AM, et al. (2008) Geochronology of igneous rocks and formation of the Late Paleozoic south Mongolian active margin of the Siberian continent. Stratigr Geol Correl 16:162-181.
45. Batulzii D, Gregory H, Amaramgalan S (2024) Evidence of Elliptical Intrusions and Sr, Hf, Pb, O Isotopes of the Khanbogd Alkali Granite Pluton: Constraction of Under-plating Magma Associated with the Duplex Thrust.
46. Zheng YF (1993) "Calculation of oxygen isotope fractionation in anhydrous silicate minerals." Geochimica et Cosmochimica Acta. 57(13):3199.
47. Holk GJ, Taylor Jr HP (2007) $^{18}O/^{16}O$ evidence for contrasting hydrothermal regimes involving magmatic and meteoric-hydrothermal waters at the Valhalla metamorphic core complex, British Columbia. Econ Geol 102(6):1063-1078.
48. Holk GJ, Taylor Jr HP (2000) Water as a petrologic catalyst driving $^{18}O/^{16}O$ homogenization and anatexis of the middle crust in the metamorphic core complexes of British Columbia. Int Geol Rev 42(2):97-130.
49. Holk GJ, Taylor Jr HP (1997) $^{18}O/^{16}O$ homogenization of the middle crust during anatexis: The Thor-Odin metamorphic core complex, British Columbia. Geology 25(1):31-34.
50. Zheng YF (1993) Calculation of oxygen isotope fractionation in hydroxyl-bearing silicates. Ear Plan Sci Lett 120(3-4):247-263.
51. Taylor HP (1988) Oxygen, hydrogen and strontium isotope constraints on the origin of granites. Earth Environ Sci Trans R Soc Edinb 79(2-3):317-338.
52. Stobbe HR (1949) Petrology of volcanic rocks of northeastern New Mexico. Geol Soc Am Bull 60(6):1041-1095.
53. Thornton CP, Tuttle OF (1960) Chemistry of igneous rocks–[Part] 1, Differentiation index. Am J Sci 258(9):664-684.
54. Verma MP, Aguilar-Y-Vargas VH, Verma SP (1986) A program package for major-element data handling and CIPW norm calculation. Comp Geosci 12(4):381-399.
55. Sun SS, McDonough WF (1989) Chemical and isotopic systematics of oceanic basalts: Implications for mantle composition and processes. Geol Soc Spec Publ 42(1):313-345.
56. Harris NB, Inger S (1992) Geochemical characteristics of pelite-derived granites. Contrib Mineral Petrol 110:46-56.
57. Woollard GP (1950) Report of the special committee on the geophysical and geological study of the continents, 1948–1949. Trans Am Geophys Union 31(1):134-142.
58. Thomson K, Petford N (2008) Structure and emplacement of high-level magmatic systems. Geological Society London
59. Wilson PI, McCaffrey KJ, Wilson RW, Jarvis I, Holdsworth RE (2016) Deformation structures associated with the Trachyte Mesa intrusion, Henry Mountains, Utah: Implications for sill and laccolith emplacement mechanisms. J Struct Geol 87:30-46.
60. Thomson K, Schofield N (2008) Lithological and structural controls on the emplacement and morphology of sills in sedimentary basins. GSL Special Publications 302: 31-44.
61. Wilson PIR, McCaffrey KJW, Wilson RW, Jarvis I, Holdsworth RE (2016) Deformation structure associated with the Trachyte Mesa intrusion, Henry Mountains, Utah: Implications for sill and laccolith emplacement mechanism. J Struct Geol 87: 30-46.
62. Ferre EC, Galland O, Montanari D, Kalakay TJ (2012) Granite magma migration and emplacement along thrusts. Int J Earth Sci 101: 1673-1688.
63. Konstantinovskaia E, Malavieille J (2005) Erosion and exhumation in accretionary orogens: Experimental and geological approaches. Geochem Geophys 6: 17-25.
64. Montanez IP, Poulsen CJ (2013) The late paleozoic ice age: An evolving paradigm. Annu Rev Earth Planet Sci 41: 629-656.
65. Gregory RT, Criss RE, Taylor HP (1989) Oxygen isotope exchange kinetics of mineral pairs in closed and open systems: Applications to problems of hydrothermal alteration of igneous rocks and Precambrian iron formations. Chem Geo 75: 1-42.
66. Hutton DHW (1992) Granite sheeted complexes: Evidence for the dyking ascent mechanism. Trans Roy Soc Edinb, Earth Sci 83: 377-382.
67. Hutton DHW (1988) Igneous emplacement in a shear zone termination: The biotite granite at Strontian, Scotland. Geol Soc Am Bull 100: 1392-1399.
68. Kato Y, Fujinaga K, Nakamura K, Takaya Y, Kitamura K, et al. (2011) Deep-sea mud in the Pacific Ocean as a potential resource for rare-earth elements. Nature Geosci 4: 534-539.
69. Milinovic J, Rodrigues FJL, Barriga FJAS, Murton BJ (2021) Ocean-floor sediments as a resource of rare earth elements: An overview of recently studied sites. Minerals 11: 142.

70. Takaya Y, Yasukawa K, Kawasaki T, Fujinaga K, Ohta J, et al. (2018) The tremendous potential of deep-sea mud as a source of rare-earth elements. Sci rep 8(1):1-8.

71. Eiler JM, Farley KA, Valley JW, Hauri E, Craig H, et al. (1997) Oxygen isotope variations in ocean island basalt phenocrysts. Geochimica et Cosmochimica Acta 61(11):2281-2293.

72. Plank T, Langmuir CH (1998) The chemical composition of subducting sediment and its consequences for the crust and mantle. Chemgeo 145(4):325-394..

73. Yasukawa K, Liu H, Fujinaga K, Machida S, Haraguchi S et al. (2014) Geochemistry and mineralogy of REY-rich mud in the eastern Indian Ocean. J Asian Earth Sci 93:25-36.

74. Wickham SM, Taylor HP. Stable isotope constraints on the origin and depth of penetration of hydrothermal fluids associated with hercynian regional metamorphism and crustal anatexis in the pyrenees. Contrib Mineral Petrol 95:255-268.

75. Blight JH, Crowley QG, Petterson MG (2010) Granites of the Southern Mongolia Carboniferous Arc: New geochronological and geochemical constraints. Lithos 116(1-2):35-52.

76. Enkhbat T, Baldorj B, Ulamsain Y, Enksaikhan Ch, Otgonbayar M (2017) Geological mapping and preliminary prospecting project at the scale of 1:50000 in Mungun Morit, Bayanjargalan areas of Tuv and Tsenhermandal, Delgerkhan areas of Khentei province.

77. Badarch G, Cunningham WD, Windley BF (2002) A new terrane subdivision for Mongolia: Implications for the phanerozoic crustal growth of Central Asia. J Asian Earth Sci 21(1):87-110.

78. Cox KG (1993) Continental magmatic underplating. Philos Trans 342(1663):155-166.

79. Fyfe WS. (1992) Magma underplating of continental crust. J Volcanol Geotherm Res 50(1-2):33-40.

80. Thybo H, Nielsen CA (2009) Magma-compensated crustal thinning in continental rift zones. Nature. 457(7231):873-876.

81. Stel H, Cloetingh SA, Heeremans M (1993) Anorogenic granites, magmatic underplating and the origin of intracratonic basins in a non-extensional setting. Tectonophysics. 226(1-4):285-299.

82. Bussien D, Gombojav N, Winkler W, Von Quadt A (2011) The Mongol–Okhotsk Belt in Mongolia—an appraisal of the geodynamic development by the study of sandstone provenance and detrital zircons. Tectonophysics 510(1-2):132-150.

83. Kovalenko VI, Kuzmin MI, Zonenshain LP, Nagibina MS, Pavlenko AS, et al. (1971) Rare metal granitoids in Mongolia: Petrology, distribution of rare elements. Transaction 5:239.

84. Tong Y, Jahn BM, Wang T, Hong DW, Smith EI, et al. (2015) Permian alkaline granites in the Erenhot–Hegenshan belt, northern Inner Mongolia, China: Model of generation, time of emplacement and regional tectonic significance. J Asian Earth Sci 97:320-36.

85. Zhang X, Gao Y, Lei S (2018) Geochronology and geochemistry of the early permian a-type granite in the Hongol area, central Inner Mongolia: Petrogenesis and tectonic implications. Acta Geologica Sinica 92(3):988-1007.

86. Zhao Z, Xiong X, Wang Q, Bai Z, Qiao Y (2009) Late paleozoic underplating in North Xinjiang: Evidence from shoshonites and adakites. Gondwana Res 16(2):216-226.

87. Othman DB, White WM, Patchett J (1989) The geochemistry of marine sediments, island arc magma genesis and crust-mantle recycling. Earth Planet Sci Lett 94(1-2):1-21.

88. Vervoort JD, Patchett PJ, Blichert-Toft J, Albarède F (1999) Relationships between Lu–Hf and Sm–Nd isotopic systems in the global sedimentary system. Earth Planet Sci Lett 168(1-2):79-99.

89. Vervoort J.D, Patchett P.J (1996) Behavior of hafnium and neodymium isotopes in the crust: Constraints from precambrian crustally derived granites. Geochim Cosmochim Acta 60: 3717-3733.